

October 31, 2018

Review of D Semi-leptonic Decays

CHUNLEI LIU¹

*Department of Physics
Carnegie Mellon University, Pittsburgh, PA, 15213*

Semi-leptonic D decays continue to play an important role in the field of flavor physics. During this presentation, recent measurements from pseudo-scalar to pseudo-scalar modes, pseudo-scalar to vector modes, and rare modes will be discussed. These results are important for many purposes, such as validating the machinery of lattice QCD, extracting CKM matrix elements, and searching for new physics and new interactions.

PRESENTED AT

The 5th International Workshop on Charm Physics
Honolulu, Hawai'i , May 14–17, 2012

¹Work supported by the Department of Energy, United States, under contract DE-FG02-91ER40682.

1 Semileptonic D Decays in the Big Picture

One important task in the field of flavor physics is to over-constrain the CKM matrix. By doing so not only will we understand better the standard model (SM) physics, but we also have the opportunity to discover new physics. To best extract CKM matrix elements, we need inputs both from experimental data and from theoretical calculations. Fig. 1 shows our best knowledge about the CKM matrix up to today[1]. Our understanding about $\sin 2\beta$ is the best thanks to clean theory and large statistics from experiments. In contrast, our understanding of both mixing and $|V_{ub}|$ have limitations from theoretical predictions.

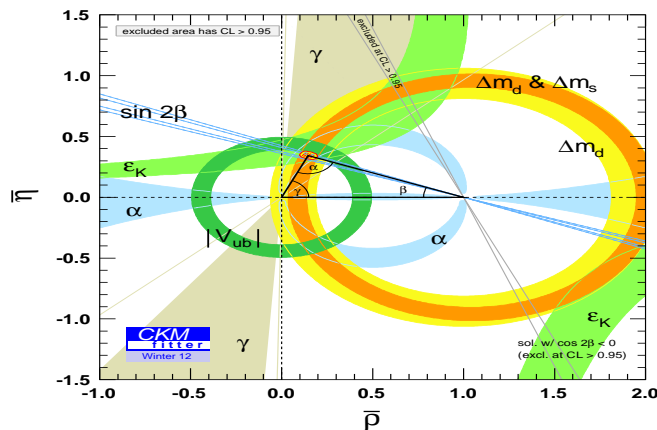


Figure 1: Constraints in the $(\bar{\rho}, \bar{\eta})$ plane. The red hashed region of the global combination corresponds to 68% C.L..

For example, $|V_{ub}|$ is measured from $B^0 \rightarrow \pi e \nu$ which has the differential decay rate as the following:

$$\frac{d\Gamma}{dq^2} = \frac{G_F^2}{24\pi^3} |V_{ub}|^2 p_\pi^3 |f_+(q^2)|^2. \quad (1)$$

In order to extract the value of $|V_{ub}|$ from the branching fraction measurement, we need information on the hadronic form factor $f_+(q^2)$. The latest world average of $|V_{ub}|$ is [1]:

$$|V_{ub}| \times 10^3 = 3.92 \pm 0.09 \pm 0.45, \quad (2)$$

where the uncertainties are from experiment and theory respectively. As we can see, the error due to theory is much larger than the experimental one. Our best understanding about $f_+(q^2)$ is from lattice QCD calculations. To validate improved lattice QCD calculations for the form factor in semi-leptonic B decays, we can use semi-leptonic D decays as a test and calibration. The differential decay rate function

for the semi-leptonic D decays is :

$$\frac{d\Gamma}{dq^2} = \frac{G_F^2}{24\pi^3} |V_{cs(d)}|^2 p_{K(\pi)}^3 |f_+(q^2)|^2 \quad (3)$$

where a massless lepton is assumed. Since the CKM matrix elements $|V_{cs(d)}|$ can be obtained precisely from unitarity, we have a reliable method to check the lattice QCD calculations.

The above example demonstrates how charm physics, in particular semi-leptonic D decays, can contribute to the larger picture of flavor physics. And more specifically, there are several advantages in using these decays:

- Key modes have large branching fractions and are experimentally easily accessible at threshold experiments (where the missing neutrino can be inferred from missing four-momentum).
- The theory of semi-leptonic decays is relatively clean, since the weak and strong interaction portions can be factored apart.
- The pseudo-scalar to pseudo-scalar decay modes provide a simple and clean way to measure the form factor. And pseudo-scalar to vector decay modes provide access to even more form factors, if desired.
- Rare semi-leptonic decays can also provide good paths to find new physics or new interactions.

2 Recent Results

The experimental results of D semi-leptonic decays can be summarized in two main categories: the exclusive decays and the inclusive decays. Several recent measurements from the exclusive semi-leptonic D decays are discussed here.

2.1 Measurements of $D \rightarrow Ke\nu$ and $D \rightarrow \pi e\nu$

As previously discussed, these channels provide constraints on lattice QCD given CKM matrix elements or vice versa, and they have been measured in many experiments such as FOCUS, Belle, BaBar and CLEO-c. The main goal currently is to improve the precision for the Cabibbo-suppressed decay $D \rightarrow \pi e\nu$.

The BESIII experiment has taken $\sim 2.9 \text{ fb}^{-1} \psi(3770)$ data during the 2010 and 2011 data runs. Using one-third of the data, a partially-blind analysis has been done with the $D^0 \rightarrow Ke\nu$ and $D^0 \rightarrow \pi e\nu$ decays. Preliminary results were first presented at this Charm 2012 conference.

2.1.1 Event Selection

The BESIII experiment takes data at the BEPCII symmetric electron-positron collider, with the $\psi(3770)$ produced at threshold. Using the double tag technique, several hadronic D decays are fully reconstructed at first. In case of multiple candidates, the candidate with minimum ΔE is chosen; ΔE is defined as

$$\Delta E \equiv E_{cand} - E_{beam}, \quad (4)$$

where E_{cand} is the energy of the reconstructed tag mode, and E_{beam} is the beam energy. The following four hadronic D decays are used: $D^0 \rightarrow K^- \pi^+$, $D^0 \rightarrow K^- \pi^+ \pi^0$, $D^0 \rightarrow K^- \pi^+ \pi^0 \pi^0$, $D^0 \rightarrow K^- \pi^+ \pi^- \pi^+$. The m_{BC} distributions of these hadronic tags with our nominal ΔE requirements are shown in Fig. 2, where the beam constrained energy m_{BC} is defined as:

$$m_{BC} \equiv \sqrt{E_{beam}^2 - |\vec{p}_{cand}|^2}, \quad (5)$$

where \vec{p}_{cand} is the momentum of the reconstructed tag mode.

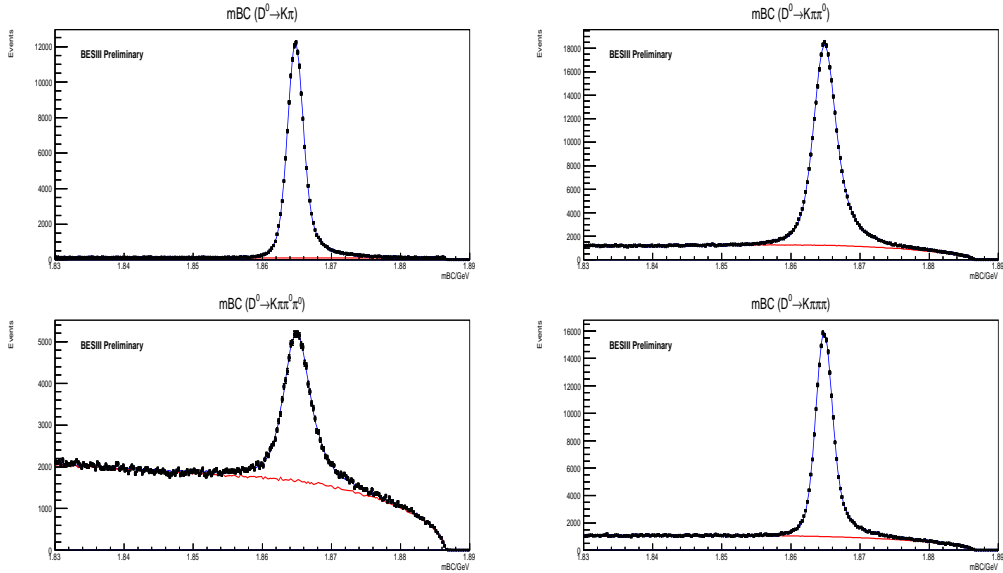


Figure 2: m_{BC} distributions of $D^0 \rightarrow K^- \pi^+$, $D^0 \rightarrow K^- \pi^+ \pi^0$, $D^0 \rightarrow K^- \pi^+ \pi^0 \pi^0$, $D^0 \rightarrow K^- \pi^+ \pi^- \pi^+$, with a ΔE cut of $\pm 3\sigma$ for modes without π^0 and -4σ to $+3\sigma$ for modes with π^0 .

After hadronic D tags are found, m_{BC} are further required to be between 1.858 GeV and 1.874 GeV before attempting to reconstruct signal candidates. The corresponding tag yields and tag efficiencies are listed in Tab. 1. To search for the signal candidates, the following requirements are applied:

Tag mode	Tag Yields	Fraction(%)	Tag efficiency
$D^0 \rightarrow K^- \pi^+$	159929 ± 413	20.7	62.08 ± 0.07
$D^0 \rightarrow K^- \pi^+ \pi^0$	323348 ± 667	41.8	33.56 ± 0.03
$D^0 \rightarrow K^- \pi^+ \pi^0 \pi^0$	78467 ± 480	10.1	14.93 ± 0.04
$D^0 \rightarrow K^- \pi^+ \pi^- \pi^+$	211910 ± 550	27.4	36.80 ± 0.04

Table 1: Tag yields and tag efficiencies using $\sim 923 \text{ pb}^{-1}$ of $\psi(3770)$ data from BESIII.

- Only two good charged tracks with opposite charges left in the event.
- One track is identified as an electron candidate, and the other track is identified as a kaon (pion) candidate for the $K^+ e^- \nu$ ($\pi^+ e^- \nu$) mode.
- The electron has the same charge as the kaon track from the tag side D .
- The candidate is vetoed if the most energetic unmatched shower has energy greater than 250 MeV, in order to suppress backgrounds with extra π^0 s.

The energy and momentum of the missing neutrino is inferred by using:

$$E_{miss} = E_{beam} - E_{hadron} - E_{electron} \quad (6)$$

$$\vec{P}_{miss} = -\vec{P}_{tag} - \vec{P}_{hadron} - \vec{P}_{electron}. \quad (7)$$

The number of signal events are obtained by fitting the $U \equiv E_{miss} - P_{miss}$ distributions. Fig. 3 shows the U distributions and fit projections for the decay of $\bar{D}^0 \rightarrow K^+ e^- \bar{\nu}$ and $\bar{D}^0 \rightarrow \pi^+ e^- \bar{\nu}$.

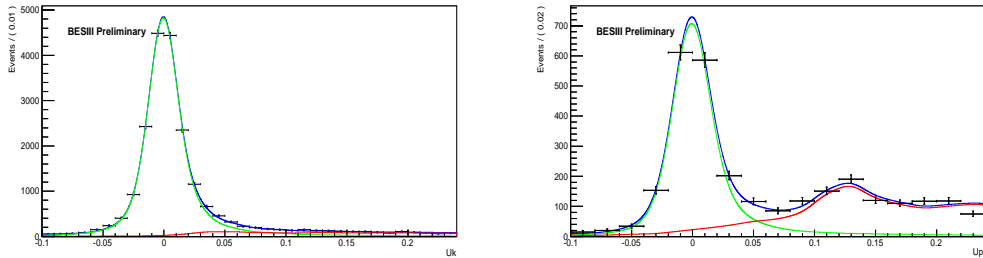


Figure 3: U distributions of $\bar{D}^0 \rightarrow K^+ e^- \bar{\nu}$ (left) and $\bar{D}^0 \rightarrow \pi^+ e^- \bar{\nu}$ (right). Blue, green, and red curves are the total fit, signal fit, and background fit, respectively.

2.1.2 Measurements of Branching Fractions and Partial Decay Rates

Given the signal yields obtained from fitting U distributions and signal efficiencies obtained from signal Monte Carlo, the branching fractions are obtained through the following equation:

$$B_{sig} = \frac{N_{sig}^{obs}}{\sum_{\alpha} N_{tag}^{obs,\alpha} \epsilon_{tag,sig}^{\alpha} / \epsilon_{tag}^{\alpha}}, \quad (8)$$

where N_{sig}^{obs} is the total number of signal yields with all tag modes combined, $N_{tag}^{obs,\alpha}$ is the observed tag yields for tag mode α , ϵ_{tag}^{α} is the tag efficiency for mode α , and $\epsilon_{tag,sig}^{\alpha}$ is the combined signal and tag efficiency for mode α . Preliminary results of branching fractions are listed in Tab. 2.

mode	Measurement(%)	PDG value (%)	CLEO-c value (%)
$\overline{D}^0 \rightarrow K^+ e^- \overline{\nu}$	$3.542 \pm 0.030 \pm 0.067$	3.55 ± 0.04	$3.50 \pm 0.03 \pm 0.04$
$\overline{D}^0 \rightarrow \pi^+ e^- \overline{\nu}$	$0.288 \pm 0.008 \pm 0.005$	0.289 ± 0.008	$0.288 \pm 0.008 \pm 0.003$

Table 2: Branching fraction measurements using $\sim 923 \text{ pb}^{-1}$ of $\psi(3770)$ data from BESIII.

In order to measure form factor, partial decay rates are measured in different q^2 bins, where q^2 is the invariant mass squared of the electron-neutrino system. $\overline{D}^0 \rightarrow K^+ e^- \overline{\nu}$ candidates are divided into nine q^2 bins (in GeV^2): $[0.0, 0.2)$, $[0.2, 0.4)$, $[0.4, 0.6)$, $[0.6, 0.8)$, $[0.8, 1.0)$, $[1.0, 1.2)$, $[1.2, 1.4)$, $[1.4, 1.6)$, $[1.6, \infty)$, while $\overline{D}^0 \rightarrow \pi^+ e^- \overline{\nu}$ are divided into seven q^2 bins: $[0.0, 0.3)$, $[0.3, 0.6)$, $[0.6, 0.9)$, $[0.9, 1.2)$, $[1.2, 1.5)$, $[1.5, 2.0)$, $[2.0, \infty)$. Signal yields in each q^2 bin are obtained by fitting U distributions in that q^2 range. Using an efficiency matrix vs. q^2 , obtained from Monte-Carlo simulation, to correct for smearing, and combining with tag yields and tag efficiencies from previous studies, the partial decay rates are obtained, as shown in Fig. 4.

With measured partial decay rates, we can also obtain the $f_+(q^2)$ at the center of each q^2 bin i using:

$$f_+(q_i^2) = \frac{1}{|V_{cd(s)}|} \sqrt{\frac{\Delta\Gamma_i}{\Delta q_i^2} \frac{24\pi^3}{G_F^2 p_i^3}}, \quad (9)$$

where $|V_{cd(s)}|$ can be taken from the PDG value, and p_i^3 is the effective value averaged over q_i^2 , calculated from:

$$p_i^3 = \frac{\int p^3 |f_+(q^2)|^2 dq^2}{\int |f_+(q^2)|^2 dq^2}, \quad (10)$$

where the three-parameter series parameterization for $f_+(q^2)$ is used from fitting data later. The $f_+(q^2)$ distributions are shown in Fig. 5 with theoretical curves overlaid [2].

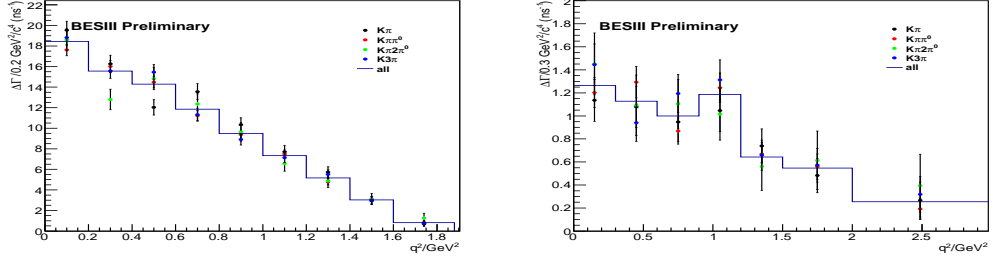


Figure 4: Partial decay rates measurement using individual tag modes (points) and all tag modes combined (histogram) for decay of $\bar{D}^0 \rightarrow K^+e^-\bar{\nu}$ (left) and $\bar{D}^0 \rightarrow \pi^+e^-\bar{\nu}$ (right).

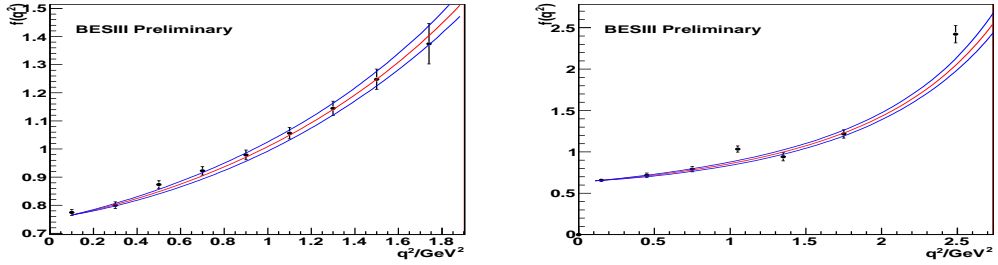


Figure 5: $f_+(q^2)$ distributions for the decay of $\bar{D}^0 \rightarrow K^+e^-\bar{\nu}$ (left) and $\bar{D}^0 \rightarrow \pi^+e^-\bar{\nu}$ (right). Points are measured from data, red curves are the theoretical predictions, and blue curves represents variations within one statistical standard sigma.

2.1.3 Measurements of the Form Factors

Three different parameterizations of the form factor $f_+(q^2)$ are considered.

The first parameterization, known as the simple pole model, is dominated by a single pole [3]:

$$f_+(q^2) = \frac{f_+(0)}{1 - q^2/m_{pole}^2}, \quad (11)$$

where the values of m_{pole} is predicted to be $M_{D_{(s)}^*}$. Note that, however, that m_{pole} is floated in the fit in addition to $f_+(0)$ to improve fit quality.

The second parameterization is known as the modified pole model [3]:

$$f_+(q^2) = \frac{f_+(0)}{\left(1 - \frac{q^2}{m_{pole}^2}\right) \left(1 - \alpha \frac{q^2}{m_{pole}^2}\right)}, \quad (12)$$

where m_{pole} is generally fixed to the $D_{(s)}^*$ mass. Both $f_+(0)$ and α are free parameters.

The third parameterization is known as the series expansion [4]. In the series expansion model, the branch cut in the complex q^2 plane is mapped onto a unit circle $|z| < 1$, where

$$z(q^2, t_0) = \frac{\sqrt{t_+ - q^2} - \sqrt{t_+ - t_0}}{\sqrt{t_+ - q^2} + \sqrt{t_+ - t_0}}, \quad (13)$$

where $t_{\pm} = (m_D \pm m_P)^2$, and t_0 is any real number smaller than t_+ . This transformation expands the form factor about $q^2 = t_0$ as:

$$f_+(q^2) = \frac{1}{P(q^2) \phi(q^2, t_0)} \sum_{k=0}^{\infty} a_k(t_0) [z(q^2, t_0)]^k, \quad (14)$$

where a_l are real coefficients, $P(q^2) = z(q^2, m_{D^*}^2)$ for kaon final states, $P(q^2) = 1$ for pion final states, and $\phi(q^2, t_0)$ is any function that is analytic outside a cut in the q^2 plane that lies along the x-axis from t_+ to ∞ . The standard choices are $t_0 = t_+(1 - (1 - t_-/t_+)^{1/2})$ and, for ϕ :

$$\phi(q^2, t_0) = \sqrt{\frac{\pi m_c^2}{3}} \left(\frac{z(q^2, 0)}{-q^2} \right)^{5/2} \left(\frac{z(q^2, t_0)}{t_0 - q^2} \right)^{-1/2} \left(\frac{z(q^2, t_-)}{t_- - q^2} \right)^{-3/4} \frac{t_+ - q^2}{(t_+ - t_0)^{1/4}} \quad (15)$$

Notice that the term $\frac{z(q^2, 0)}{-q^2}$ has a limit of $1/(4t_+)$ as q^2 goes to zero.

With the above parameterization, the data is fitted by minimizing this χ^2 function:

$$\chi^2 = \sum_{i,j=1}^n (\Delta\Gamma_i - \Delta G_i) C_{ij}^{-1} (\Delta\Gamma_j - \Delta G_j), \quad (16)$$

where $\Delta\Gamma_i$ is the measured partial decay rate in q^2 bin i , ΔG_i is the predicted partial decay rate in q^2 bin i , and C is the covariance matrix of the measured partial decay rates. The fitted results are listed in Tab. 3.

2.2 Measurement of $D^+ \rightarrow K^- \pi^+ e^+ \nu_e$

The $D^+ \rightarrow K^- \pi^+ e^+ \nu$ decay includes contributions from different $K\pi$ resonances, including the dominant $\overline{K}^*(892)^0$ piece, as well as a non-resonant amplitude. The measurement of the $\overline{K}^*(892)^0$ (lowest vector meson) contribution can be used to study hadronic transition form factors. Using 347.5 fb^{-1} of data recorded at the $\Upsilon(4S)$ the BaBar collaboration has analyzed this decay channel [5]. In addition to measuring the form factors, a comprehensive analysis of many other items is also performed. These include the properties of the $\overline{K}^*(892)^0$ meson, the S -wave contribution to the decay, the variations of the $K\pi$ S -wave phase versus the $K\pi$ mass, and a search for radially excited P -wave and D -wave $K\pi$ resonances.

The formalism of the differential decay partial width is taken from Ref. [6], which necessarily includes five variables:

Simple Pole	$f_+(0) V_{cd(s)} $	m_{pole}	
$\overline{D}^0 \rightarrow K^+e^-\nu$	$0.729 \pm 0.005 \pm 0.007$	$1.943 \pm 0.025 \pm 0.003$	
$\overline{D}^0 \rightarrow \pi^+e^-\nu$	$0.142 \pm 0.003 \pm 0.001$	$1.876 \pm 0.023 \pm 0.004$	
Modified Pole	$f_+(0) V_{cd(s)} $	α	
$\overline{D}^0 \rightarrow K^+e^-\nu$	$0.725 \pm 0.006 \pm 0.007$	$0.265 \pm 0.045 \pm 0.006$	
$\overline{D}^0 \rightarrow \pi^+e^-\nu$	$0.140 \pm 0.003 \pm 0.002$	$0.315 \pm 0.071 \pm 0.012$	
2 par. series	$f_+(0) V_{cd(s)} $	r_1	
$\overline{D}^0 \rightarrow K^+e^-\nu$	$0.726 \pm 0.006 \pm 0.007$	$-2.034 \pm 0.196 \pm 0.022$	
$\overline{D}^0 \rightarrow \pi^+e^-\nu$	$0.140 \pm 0.004 \pm 0.002$	$-2.117 \pm 0.163 \pm 0.027$	
3 par. series	$f_+(0) V_{cd(s)} $	r_1	r_2
$\overline{D}^0 \rightarrow K^+e^-\nu$	$0.729 \pm 0.008 \pm 0.007$	$-2.179 \pm 0.355 \pm 0.053$	$4.539 \pm 8.927 \pm 1.103$
$\overline{D}^0 \rightarrow \pi^+e^-\nu$	$0.144 \pm 0.005 \pm 0.002$	$-2.728 \pm 0.482 \pm 0.076$	$4.194 \pm 3.122 \pm 0.448$

Table 3: Fitter parameters from form factor measurements for $\overline{D}^0 \rightarrow K^+e^-\nu$ and $\overline{D}^0 \rightarrow \pi^+e^-\nu$.

- m^2 , the squared mass of the kaon-pion system;
- q^2 , the squared mass of the electron-neutrino system;
- $\cos(\theta_K)$, where θ_K is the angle between the kaon three-momentum in the kaon rest frame and the line of flight of the kaon-pion system in the D rest frame;
- $\cos(\theta_e)$, where θ_e is the angle between the electron three-momentum in the electron-neutrino rest frame and the line of flight of the electron-neutrino system in the D rest frame;
- χ , the angle between the normals to the planes defined in the D rest frame by the $K\pi$ pair and the $e\nu$ pair.

2.2.1 Event Selection

To reconstruct D^+ decays, all the charged and neutral particles are boosted to the center-of-mass system and the event thrust axis is determined. A plane perpendicular to this axis defines two hemispheres, and the candidate hemisphere consists of a positron, a charged kaon, and a charged pion. A vertex fit is performed and events with probability larger than 10^{-7} are kept. To estimate the neutrino momentum, the $K^-\pi^+e^+\nu_e$ system is constrained to the D^+ mass with estimates of the D^+ direction and neutrino energy obtained from all tracks and unmatched showers measured in the event. The neutrino energy is evaluated by subtracting from the hemisphere energy

the energy of reconstructed particles contained in that hemisphere. To further reject $B\bar{B}$ background and continuum background (arising mainly from charm particles), Fisher discriminants are created from relevant variables. This discriminant retains 40% of signal events and rejects 94% of the remaining background. About 244×10^3 signal events are selected with a final signal-to-background ratio of 2.3.

2.2.2 Measurement of Form Factors and $\bar{K}^*(892)^0$ Properties

Form factors $F_{1,2,3}$ can be expanded into partial waves to show explicit dependence on θ_K . Considering only S , P and D waves, this gives:

$$\begin{aligned}
 F_1 &= F_{10} + F_{11} \cos\theta_K + F_{12} \frac{3\cos^2\theta_K - 1}{2} \\
 F_2 &= \frac{1}{\sqrt{2}} F_{21} + \sqrt{\frac{3}{2}} F_{22} \cos\theta_K \\
 F_3 &= \frac{1}{\sqrt{2}} F_{31} + \sqrt{\frac{3}{2}} F_{32} \cos\theta_K
 \end{aligned}
 \tag{17}$$

where F_{10} characterizes the S -wave contribution, and F_{i1} and F_{i2} correspond to the P - and D -waves, respectively. It is also possible to relate these form factors with the helicity form factors $H_{0,\pm}$, which can be in turn related to the two axial-vector form factors $A_{1,2}(q^2)$ and the vector form factor $V(q^2)$. For the q^2 dependence, the simple pole parameterization is used:

$$\begin{aligned}
 V(q^2) &= \frac{V(0)}{1 - q^2/m_V^2}, \\
 A_1(q^2) &= \frac{A_1(0)}{1 - q^2/m_A^2}, \\
 A_2(q^2) &= \frac{A_2(0)}{1 - q^2/m_A^2},
 \end{aligned}
 \tag{18}$$

where m_V and m_A are expected to be close to $m_{D_s^*} = 2.1$ GeV and $m_{D_{s1}} = 2.5$ GeV, respectively. In the analysis, ratios of these form factors, evaluated at $q^2 = 0$, $r_V = V(0)/A_1(0)$ and $r_2 = A_2(0)/A_1(0)$ are measured by studying the variation of partial decay rate versus kinematic variables; m_A is allowed to fit while m_V is fixed. For the mass dependence, in case of the $K^*(892)$, a Breit-Wigner distribution is used.

Tab. 4 shows the fit results considering three different models:

- $S + \bar{K}^*(892)^0$, a signal made of the $\bar{K}^*(892)^0$ and S -wave components.
- $S + \bar{K}^*(892)^0 + \bar{K}^*(1410)^0$, a signal made of the $\bar{K}^*(892)^0$, $\bar{K}^*(1410)^0$, and S -wave components.

- $S + \bar{K}^*(892)^0 + \bar{K}^*(1410)^0 + D$, a signal made of the $\bar{K}^*(892)^0$, $\bar{K}^*(1410)^0$, S - and D -wave components.

The fractions of signal components in different models are measured and shown in Tab. 5. The second model is considered as the nominal fit to data, with systematics error also listed in the table.

Variable	$S + \bar{K}^*(892)^0$	$S + \bar{K}^*(892)^0$ $\bar{K}^*(1410)^0$	$S + \bar{K}^*(892)^0$ $\bar{K}^*(1410)^0 + D$
$m_{K^*(892)}$ (MeV)	894.77 ± 0.08	$895.4 \pm 0.2 \pm 0.2$	895.27 ± 0.21
$\Gamma_{K^*(892)}^0$ (MeV)	45.78 ± 0.23	$46.5 \pm 0.3 \pm 0.2$	46.38 ± 0.26
r_{BW} (GeV^{-1})	3.71 ± 0.22	$2.1 \pm 0.5 \pm 0.5$	2.31 ± 0.20
m_A (GeV)	2.65 ± 0.10	$2.63 \pm 0.10 \pm 0.13$	2.58 ± 0.09
r_V	1.458 ± 0.016	$1.463 \pm 0.017 \pm 0.031$	1.471 ± 0.016
r_2	0.804 ± 0.020	$0.801 \pm 0.020 \pm 0.020$	0.786 ± 0.020

Table 4: Values of form factor and $\bar{K}^*(892)^0$ parameters with different models.

Component	$S + \bar{K}^*(892)^0$	$S + \bar{K}^*(892)^0$ $\bar{K}^*(1410)^0$	$S + \bar{K}^*(892)^0$ $\bar{K}^*(1410)^0 + D$
S -wave	$5.62 \pm 0.14 \pm 0.13$	$5.79 \pm 0.16 \pm 0.15$	$5.69 \pm 0.16 \pm 0.15$
P -wave	94.38	94.21	94.12
$\bar{K}^*(892)^0$	94.38	$94.11 \pm 0.74 \pm 0.75$	$94.41 \pm 0.15 \pm 0.20$
$\bar{K}^*(1410)^0$	0	$0.33 \pm 0.13 \pm 0.19$	$0.16 \pm 0.08 \pm 0.14$
D -wave	0	0	$0.19 \pm 0.09 \pm 0.09$

Table 5: Fractions (in percent) of signal components with different models.

2.2.3 Measurement of S -wave Phase

Using the nominal signal model containing S -wave, $\bar{K}^*(892)^0$ and $\bar{K}^*(1410)^0$ components, the phase in the mass-dependent S -wave amplitude is measured and compared to LASS measurements. The S -wave phase is assumed to be a constant within each of the considered $K\pi$ mass intervals. The measurement of phase variation is shown in Fig. 6.

2.3 Measurement of $D^0/D^+ \rightarrow \rho e \nu$ and $D^+ \rightarrow \omega e \nu$

Using 818 pb^{-1} of data taken at the $\psi(3770)$, the CLEO-c collaboration has measured branching fraction and form factor for the decays of $D^0/D^+ \rightarrow \rho e \nu$ and the branching

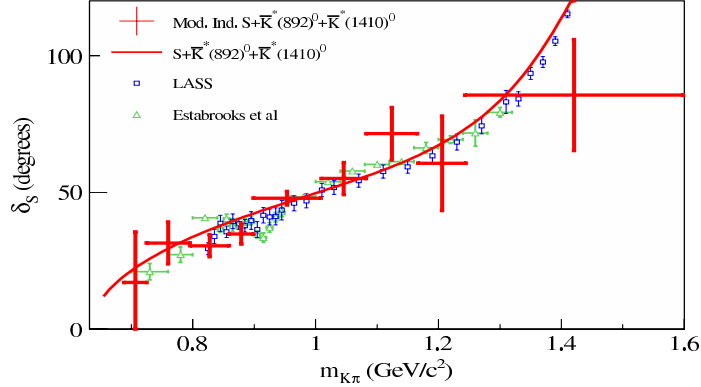


Figure 6: Points (crosses) give the S -wave phase variation using the nominal model. The phase is assumed to be constant within each mass bin, and parameters of the $\bar{K}^*(892)^0$ are fixed to values from the nominal fit to data. The solid line corresponds to the parameterized S -wave phase variation in the nominal fit. LASS data are shown in blue.

fraction for $D^+ \rightarrow \omega e \nu$ [7]. The precision of the branching fractions is improved, and the form factor result of the $D^0/D^+ \rightarrow \rho e \nu$ is the first measurement on the Cabibbo-suppressed pseudo-scalar meson to vector meson transition in semi-leptonic D decay.

2.3.1 Event Selection

The double-tag technique is used in this analysis by reconstructing a D tag in the following hadronic final states: $K^+\pi^-$, $K^+\pi^-\pi^0$, and $K^+\pi^-\pi^-\pi^+$ for neutral tags, and $K_s^0\pi^-$, $K^+\pi^-\pi^-$, $K_s^0\pi^-\pi^0$, $K^+\pi^-\pi^-\pi^0$, $K_s^0\pi^-\pi^-\pi^+$, and $K^-K^+\pi^-$ for charged tags. In case of multiple candidates in the same tag mode, the candidate with minimum ΔE is chosen. Once a tag is identified, certain ΔE and m_{BC} cuts are required. The unused tracks and showers are then searched for a candidate e^+ along with a $\rho^-(\pi^-\pi^0)$, $\rho^0(\pi^+\pi^-)$, or $\omega(\pi^+\pi^-\pi^0)$. The ρ candidate is required to have invariant mass within 150 MeV from the nominal PDG mass. The combined tag and semi-leptonic candidates must account for all reconstructed tracks and unmatched showers in the event. To remove multiple candidates in each semi-leptonic mode, one combination is chosen per tag mode per tag charge, based on the proximity of the invariant masses of the ρ^0 , ρ^+ or ω candidates to their PDG masses. The number of semi-leptonic decays are obtained by fitting the $U \equiv E_{miss} - |\vec{p}_{miss}|$ distributions, where E_{miss} and \vec{p}_{miss} are energy and momentum of the missing neutrino, and they can be inferred from all other measured particles. The U distributions are shown in Fig. 7.

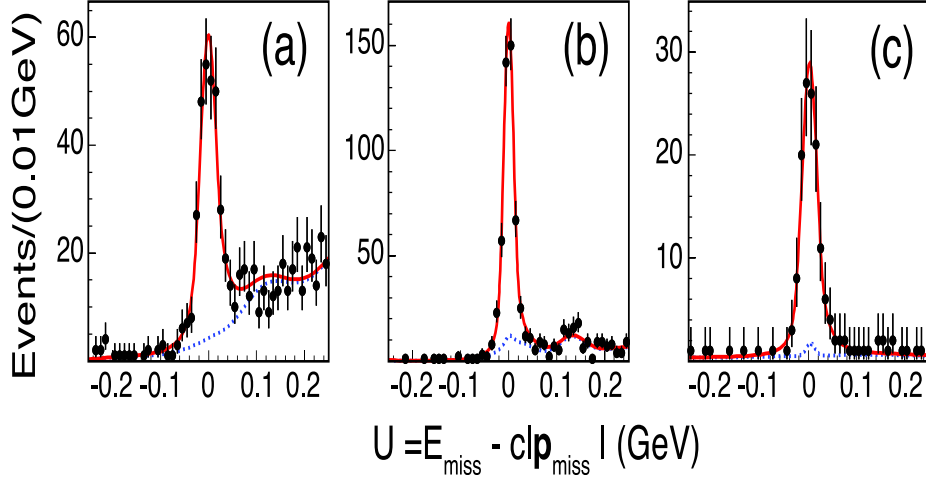


Figure 7: U distributions of (a) $D^0 \rightarrow \rho^- e^+ \nu_e$, (b) $D^+ \rightarrow \rho^0 e^+ \nu_e$ and (c) $D^+ \rightarrow \omega e^+ \nu_e$.

2.3.2 Measurements of Branching Fraction

To measure the absolute branching fraction, Monte-Carlo samples are used to determine tag and signal efficiencies. Together with the tag and signal yields, the same equation as Eq. 8 can be used to give the branching fraction. The measured results are listed in Tab. 6.

Decay mode	$\epsilon(\%)$	N_{sig}	B_{SL}	$B_{SL}(\text{ISGW2})$	$B_{SL}(\text{FK})$
$D^0 \rightarrow \rho^- e^+ \nu_e$	26.03 ± 0.02	304.6 ± 20.9	$1.77 \pm 0.12 \pm 0.10$	1.0	2.0
$D^+ \rightarrow \rho^0 e^+ \nu_e$	42.84 ± 0.03	447.4 ± 24.5	$2.17 \pm 0.12_{-0.22}^{+0.12}$	1.3	2.5
$D^+ \rightarrow \omega e^+ \nu_e$	14.67 ± 0.03	128.5 ± 12.6	$1.82 \pm 0.18 \pm 0.07$	1.3	2.5

Table 6: Branching fractions for $D^0 \rightarrow \rho^- e^+ \nu_e$, $D^+ \rightarrow \rho^0 e^+ \nu_e$ and $D^+ \rightarrow \omega e^+ \nu_e$, from the CLEO-c analysis and two model predictions: ISGW2[8] and FK[9]. The uncertainties for signal efficiency ϵ and signal yields N_{sig} are statistical only. The efficiency includes the ρ and ω branching fractions from the PDG.

2.3.3 Measurements of Form Factor

A form factor analysis is performed for $D^0/D^+ \rightarrow \rho^-/\rho^0 e^+ \nu_e$ decays. The mechanism of this decay is similar to the $D^+ \rightarrow K\pi e\nu$ discussed in Sec. 2.2, except only P -wave is considered in this case. Three dominant form factors, two axial and one vector, A_1 , A_2 , and V , are used to describe the hadronic current. A simple pole model is assumed with the pole mass fixed as $M_{D^*(1^-)} = 2.01$ GeV and $M_{D^*(1^+)} = 2.42$ GeV for the vector and axial form factors, respectively. A four-dimensional maximum likelihood

fit [10] is performed in the space of q^2 , $\cos\theta_\pi$, $\cos\theta_e$ and χ , and a simultaneous fit is made to the isospin-conjugate modes $D^0 \rightarrow \rho^0 e^+ \nu_e$ and $D^+ \rightarrow \rho^- e^+ \nu_e$. The ratios of form factors evaluated at $q^2 = 0$, $r_V = \frac{V(0)}{A_1(0)}$ and $r_2 = \frac{A_2(0)}{A_1(0)}$ are obtained: $r_V = 1.48 \pm 0.15 \pm 0.05$ and $r_2 = 0.83 \pm 0.11 \pm 0.04$. Using $|V_{cd}| = 0.2252 \pm 0.0007$, $\tau_{D^0} = (410.1 \pm 1.5) \times 10^{-15}$ s, and $\tau_{D^+} = (1040 \pm 7) \times 10^{-15}$ s, from PDG 2010, form factor ratios and branching fraction results are combined to obtain : $A_1(0) = 0.56 \pm 0.01_{-0.03}^{+0.02}$, $A_2(0) = 0.47 \pm 0.06 \pm 0.04$, and $V(0) = 0.84 \pm 0.09_{-0.06}^{+0.05}$. The fit projection is shown in Fig. 8, where the difference between data and the fit projection for $\cos\theta_\pi$ may be due to S -wave interference.

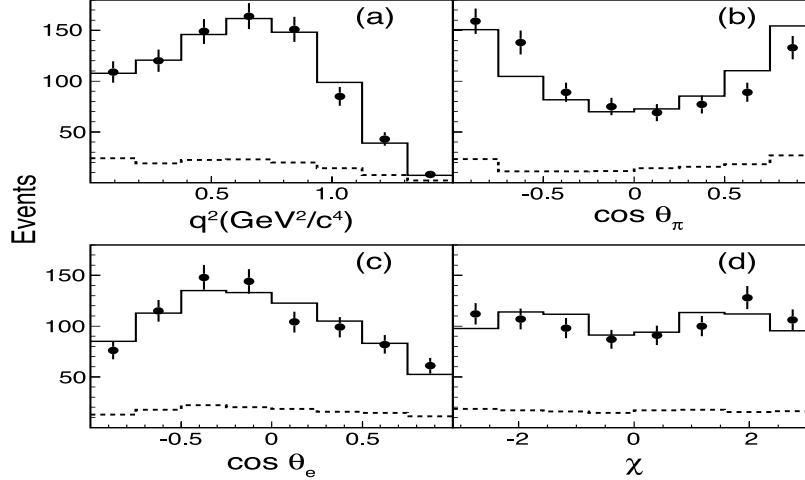


Figure 8: Projections of the combined ρ^- and ρ^0 data (points with statistics error bar) and the fit (solid histogram). The dashed lines show the background distributions.

2.4 Search for the Decay of $D_s^+ \rightarrow \omega e^+ \nu$

Using data collected at a center-of-mass energy $\sqrt{s} = 4170$ MeV, CLEO-c searched for the decay of $D_s^+ \rightarrow \omega e^+ \nu$, which can probe the four-quark content of the D_s^+ [11]. The integrated luminosity of the data used in this analysis is 586 pb^{-1} , or 0.6×10^6 $D_s^+ D_s^-$ inclusive decays. Recent work by Gronau and Rosner [12] concludes that any value of the branching fraction for $D_s^+ \rightarrow \omega e^+ \nu$ exceeding 2×10^{-4} is unlikely to be from $\omega - \phi$ mixing.

2.4.1 Event Selection

About 95% of the $e^+ e^- \rightarrow D_s^+ X$ events are formed from the following exclusive reactions [13]:

$$e^+ e^- \rightarrow D_s^+ D_s^{*-}, \quad e^+ e^- \rightarrow D_s^- D_s^{*+}, \quad (19)$$

with equal amounts of them produced, and about 95% of the D_s^* decays through $D_s\gamma$,

To select signal events, the double tag technique is used. Eight D_s tag modes are reconstructed: $K_s^0 K^-$, $K^+ K^- \pi^-$, $K^{*-} \bar{K}^{*0}$, $\pi^+ \pi^- \pi^-$, $\eta \pi^-$, $\eta \rho^-$, $\pi^- \eta'(\eta \pi^+ \pi^-)$, $\pi^- \eta'(\rho \gamma)$. The four-momentum of a tag candidate is defined by (E_{tag}, \vec{p}_{tag}) , and the recoil mass M_{rec} is defined as

$$M_{rec} = \sqrt{(E_b - E_{tag})^2 - (\vec{p}_b - \vec{p}_{tag})^2}, \quad (20)$$

where (E_b, \vec{p}_b) is the four-momentum of the colliding beams. The M_{rec} distribution peaks at zero only for events where the photon is associated with signal side, but even if the photon is associated with the tag side, M_{rec} is kinematically constrained such that $|M_{rec} - M_{D_s^*}| < 55$ MeV. So only events passing with this wide cut are retained. The distribution of invariant mass of the tag M_{tag} is fitted with a double Gaussian function, and the weighted resolution σ is used to define signal regions. All tag modes are required to be within 2.5σ from the peak position except for the $\eta\rho$ mode where it is selected with 2σ . A second kinematic constraint is used, on the MM^{*2} defined as

$$MM^{*2} = (E_b - E_{tag} - E_\gamma)^2 - (\vec{p}_b - \vec{p}_{tag} - \vec{p}_\gamma)^2, \quad (21)$$

where MM^{*2} is expected to peak at $M_{D_s}^2$ (independent of whether the γ is from the tag or signal side). The selection criteria on MM^{*2} is determined from a two-dimensional binned likelihood fit the (MM^{*2}, M_{tag}) space.

The signal is then selected by requiring one positron candidate with charge opposite to the tag charge, two charged pions of opposite charges, and no extra good tracks. A yet-unused good π^0 candidate is also required. There can be multiple π^0 candidates; if so, the one with lowest $\chi^2 = [(M_{\gamma\gamma} - M_{\pi^0})/\sigma_{\gamma\gamma}]^2$ is chosen, where $M_{\gamma\gamma}$ is the photon-photon mass, and $\sigma_{\gamma\gamma}$ is the calculated resolution. The positron, charged pions, and π^0 are added together to get a four-vector (E_s, \vec{p}_s) . With information from beams and tag side, the missing-mass squared of the neutrino is obtained:

$$MM^2 = (E_b - E_{tag} - E_\gamma - E_s)^2 - (\vec{p}_b - \vec{p}_{tag} - \vec{p}_\gamma - \vec{p}_s)^2. \quad (22)$$

2.4.2 Final Fit and Results

To extract the signal yields, the mass of the $\pi^+ \pi^- \pi^0$ system, M_3 , is used with a cut on MM^2 as $-0.05 < MM^2 < 0.05$ GeV². The M_3 distribution is shown in Fig. 9, where one can see peaks for the η and ϕ , but no clear signal peak at the ω . An upper limit on the branching fraction of $B(D_s^+ \rightarrow \omega e^+ \nu) < 0.20\%$ is obtained at 90% confidence level.

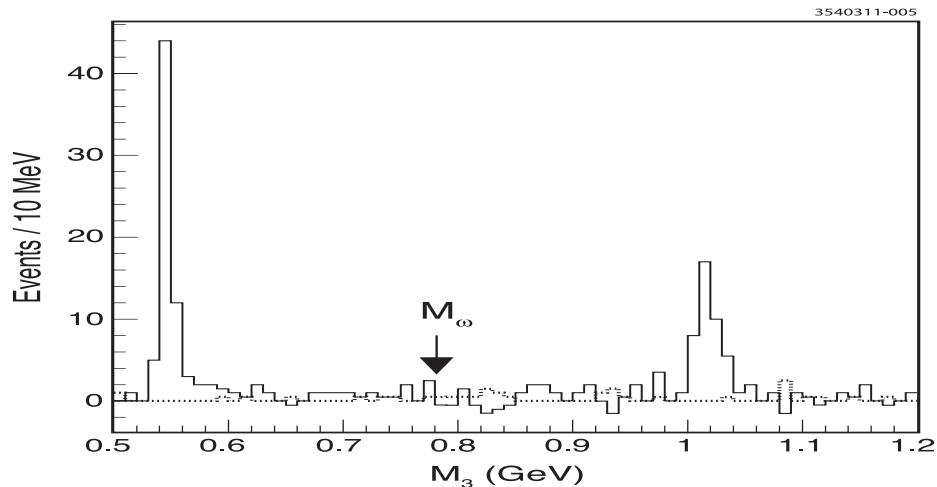


Figure 9: M_3 ($M(3\pi)$ distribution. Solid line: signal selection, after M_{tag} sideband subtraction. Dotted line: M_{tag} sideband contribution.

3 Summary

Experimental measurements of semi-leptonic D decays have been studied very successful during the past few years, with contributions from experiments such as FOCUS, Belle, BaBar and CLEO-c. During this presentation, recent results on semi-leptonic D decays have been discussed, with topic covering several topical aspects, i.e., pseudo-scalar to pseudo-scalar modes, pseudo-scalar to vector modes, and rare modes.

Since the start of running in 2008, the newest of these experiments, BESIII, has taken about 2.9 fb^{-1} of data at $\psi(3770)$. With peak luminosity reaching more than 6×10^{32} (60% of the designed luminosity), BESIII is poised to take more data at $\psi(3770)$ and in the higher D_s energy region. Using part of the data, BESIII has presented preliminary results of the $D^0 \rightarrow K/\pi e \nu$ decays. Results from the full dataset and other modes are coming in the near future.

ACKNOWLEDGEMENTS

The author thanks Charm 2012 committee for the invitation to the conference and their great organization.

References

- [1] CKMfitter group, preliminary results as of Winter 2012.

- [2] Jon A. Bailey *et al.*, “D semileptonic form factors and $-V_{cs}(d)-$ from 2+1 flavor lattice QCD”, arXiv:1111.5471.
- [3] D. Becirevic and A. B. Kaidalov, Phys. Lett. B **478**, 417 (2000).
- [4] T. Becher and R. J. Hill, Phys. Lett. B **633**, 61 (2006).
- [5] P. del Amo Sanchez *et al.* (BaBar Collaboration), Phys. Rev. D **83**, 072001 (2011).
- [6] C. L. Y. Lee, M. Lu, and M. B. Wise, Phys. Rev. D **46**, 5040 (1992).
- [7] S. Dobbs *et al.* [CLEO Collaboration], arXiv:1112.2884 [hep-ex].
- [8] D. Scora and N. Isgur, Phys. Rev. D **52**, 2783 (1995).
- [9] S. Fajfer and J. Kamenik, Phys. Rev. D **72**, 034029 (2005).
- [10] D. M. Schmidt, R. J. Morrison and M. S. Witherell, Nucl. Instrum. Meth. A **328**, 547 (1993).
- [11] L. Martin *et al.* (CLEO Collaboration), Phys. Rev. D **84**, 012005 (2011).
- [12] M. Gronau and J. L. Rosner, Phys. Rev. D **79** 074006 (2009).
- [13] D. Cronin-Hennessy *et al.* (CLEO Collaboration), Phys. Rev. D **80** 072001 (2009).